J Solid State Electrochem (2012) 16:1229–1237
DOI 10.1007/s10008-011-1513-6

ORIGINAL PAPER

Influence of Li source on tap density and high rate cycling performance of spherical $Li[Ni_{1/3}Co_{1/3}Mn_{1/3}]O_2$ for advanced lithium-ion batteries

Shunyi Yang · Xianyou Wang · Xiukang Yang · Li Liu · Ziling Liu · Yansong Bai · Yingping Wang

Received: 9 June 2011 / Revised: 20 July 2011 / Accepted: 23 July 2011 / Published online: 17 August 2011

Abstract Spherical $Li[Ni_{1/3}Co_{1/3}Mn_{1/3}]O_2$ cathode materials with different microstructure have been prepared by a continuous carbonate co-precipitation method using $LiOH{\cdot}H_2O$, Li_2CO_3, $CH_3COOLi{\cdot}2H_2O$ and $LiNO_3$ as lithium source. The effects of Li source on the physical and electrochemical properties of $Li[Ni_{1/3}Co_{1/3}Mn_{1/3}]O_2$ are investigated by X-ray diffraction (XRD), scanning electron microscopy (SEM) and electrochemical measurements. The results show that the morphology, tap density and high rate cycling performance of $Li[Ni_{1/3}Co_{1/3}Mn_{1/3}]O_2$ spherical particles are strongly affected by Li source. Among the four Li sources used in this study, $LiOH{\cdot}H_2O$ is beneficial to enhance the tap density of $Li[Ni_{1/3}Co_{1/3}Mn_{1/3}]O_2$, and the tap density of as-prepared sample reaches 2.32 $g cm^{-3}$. Meanwhile, Li_2CO_3 is preferable when preparing the $Li[Ni_{1/3}Co_{1/3}Mn_{1/3}]O_2$ with high rate cycling performance, upon extended cycling at 1 and 5C rates, 97.5% and 92% of the initial discharge capacity can be maintained after 100 cycles.

Key words Lithium ion batteries · $Li[Ni_{1/3}Co_{1/3}Mn_{1/3}]O_2$ · Li source · Carbonate co-precipitation · Tap density · Cycling performance

Introduction

In recent years, the lithium transition metal oxides $Li[Ni_xCo_{1-2x}Mn_x]O_2$ $(0 \le x \le 0.5)$ as cathode materials for lithium-ion batteries have been of great interest and potential candidates to replace the commercial $LiCoO_2$. These include $Li[Ni_{1/2}Mn_{1/2}]O_2$ [1], $Li[Ni_{1/3}Co_{1/3}Mn_{1/3}]O_2$ [2–4], and $Li[Ni_{0.4}Co_{0.2}Mn_{0.4}]O_2$ [5, 6]. The electrochemical processes involve the redox pair of Ni^{2+}/Ni^{4+} with two-electron transfer in the series of these compounds. Among them, $Li[Ni_{1/3}Co_{1/3}Mn_{1/3}]O_2$ has been studied extensively as a promising cathode material for lithium-ion batteries as it exhibits much higher capacity, structural stability and enhanced safety [7, 8]. However, to replace the commercial $LiCoO_2$ as a cathode material for advanced lithium ion batteries, which required high energy density and high power density, the tap density and high rate cycling performance of the $Li[Ni_{1/3}Co_{1/3}Mn_{1/3}]O_2$ must be further improved [9–12]. Recently, Li sources have proved to be an important factor in influencing the grain size and rate capability of $LiNi_{1-y}Co_yO_2$ [13], $LiFePO_4$ [14] and spinel $LiNi_{0.5}Mn_{1.5}O_4$ [15]. Nevertheless, to the best of our knowledge, the influences of Li source on the characteristics of $Li[Ni_{1/3}Co_{1/3}Mn_{1/3}]O_2$ have barely been reported.

$Li[Ni_{1/3}Co_{1/3}Mn_{1/3}]O_2$ can be prepared using different methods: solid-state reaction [16], sol–gel process [17], co-precipitation method [18–24], microwave method [25], rheological phase method [26] and microemulsion method [27], etc. Among these methods, co-precipitation is recognized as a promising production technique in homogeneously mixing all reagents at atomic or molecular level, allowing careful control of the stoichiometric amount, morphology and particle size distribution of the final product $Li[Ni_{1/3}Co_{1/3}Mn_{1/3}]O_2$ [18, 19]. In our previous work [24], the carbonate co-precipitation method, in which NH_4HCO_3 was used as a complexant, had been used for preparing spherical $[Ni_{1/3}Co_{1/3}Mn_{1/3}]CO_3$ as the precursor of spherical $Li[Ni_{1/3}Co_{1/3}Mn_{1/3}]O_2$ with good electrochemical performance. In this paper, a

S. Yang · X. Wang (✉) · X. Yang · L. Liu · Z. Liu · Y. Bai · Y. Wang
Key Laboratory of Environmentally Friendly Chemistry and Applications of Ministry of Education, School of Chemistry, Xiangtan University,
Hunan, Xiangtan 411105, China
e-mail: wxianyou@yahoo.com

continuous carbonate co-precipitation has been used to prepare uniform spherical $[Ni_{1/3}Co_{1/3}Mn_{1/3}]CO_3$ precursor, then the precursor was mixed with different Li sources such as $LiOH{\cdot}H_2O$, Li_2CO_3, $CH_3COOLi{\cdot}2H_2O$ and $LiNO_3$ to synthesize spherical $Li[Ni_{1/3}Co_{1/3}Mn_{1/3}]O_2$. The effects of Li source on the physical characteristics and electrochemical properties of $Li[Ni_{1/3}Co_{1/3}Mn_{1/3}]O_2$ are systematically studied.

Experimental

Preparation of spherical precursor

Spherical $[Ni_{1/3}Co_{1/3}Mn_{1/3}]CO_3$ was synthesized by a continuous carbonate co-precipitation. Details of the preparation procedures are described in a previous work [24]. The main difference between this experiment and our previous work is that two reaction vessels with the same structure are used in order to control the morphology of the precursor. One reaction vessel is used for the co-precipitation reaction, and another is used for the ageing process, which will prolong the average residence time of reaction particle in the vessel and obtain a uniform $[Ni_{1/3}Co_{1/3}Mn_{1/3}]CO_3$ precursor with perfect sphericity roundness. The obtained $[Ni_{1/3}Co_{1/3}Mn_{1/3}]CO_3$ precursor was pre-heated at 500 °C for 5 h to decompose the carbonate into an oxide compound $[Ni_{1/3}Co_{1/3}Mn_{1/3}]_3O_4$ precursor. After pre-heating, EDTA titration was used to analyze the exact amount of transition metal ions in the $[Ni_{1/3}Co_{1/3}Mn_{1/3}]_3O_4$ powder.

Preparation of spherical $Li[Ni_{1/3}Co_{1/3}Mn_{1/3}]O_2$ using different Li sources

To synthesize $Li[Ni_{1/3}Co_{1/3}Mn_{1/3}]O_2$ material, the obtained $[Ni_{1/3}Co_{1/3}Mn_{1/3}]_3O_4$ precursor was mixed thoroughly with 6% excess amounts of lithium compound by agitating in a wet batch mixer using ethanol as medium. The mixture was preheated at 500 °C for 5 h and then calcined at 900 °C for 12 h in air to obtain $Li[Ni_{1/3}Co_{1/3}Mn_{1/3}]O_2$. Hereafter, the products prepared from $LiOH{\cdot}H_2O$, Li_2CO_3, $CH_3COOLi{\cdot}2H_2O$ and $LiNO_3$ are denoted as sample A, sample B, sample C and sample D, respectively.

Structure and morphology characterization

The chemical compositions of the resulting powders were analyzed by atomic absorption spectroscopy (AAS, Vario 6 Analytik Jena AG, Jena, Germany). The tap density of sample was determined by Powder Integrative Characteristic Tester (BT-1000, Bettersize Instruments Ltd, China). The phase identification of the samples was performed with a diffractometer (D/Max-3C, Rigaku, Japan) using Cu Kα radiation (λ=1.54178 Å) and a graphite monochromator at 36 kV, 20 mA. The scanning rate was 8° min^{-1} and the scanning range of diffraction angle (2θ) was $10° \le 2\theta \le 80°$. The morphology of the sample was observed using scanning electron microscopy (SEM, JSM-5600LV, JEOL, Japan).

Electrochemical measurements

Electrochemical tests were examined using CR2025 coin-type cells. In all cells, the cathode consisted of a mixture of active material (80 wt.%), acetylene black (10 wt.%), graphite (5 wt.%) and polyvinylidene fluoride (5 wt.%) as binder agent. Lithium was used as counter and reference electrodes, a Celgard 2400 was used as separator, and the electrolyte was a 1 M $LiPF_6$ solution in ethylene carbonate (EC)-dimethyl carbonate (DMC) (1:1, v/v). Charge–discharge measurement was carried out in Neware battery test system BTS-XWJ-6.44S-00052 (Newell, Shenzhen, China). The electrochemical impedance spectroscopy (EIS) of the cells was measured on a CHI 660A electrochemical workstation (Chenhua, China) in the frequency range of 10 kHz–10 MHz with an AC voltage of 5 mV.

Results and discussion

Through the continuous carbonate co-precipitation process, pink-colored $[Ni_{1/3}Co_{1/3}Mn_{1/3}]CO_3$ powder was obtained. The X-ray diffraction (XRD) pattern of the $[Ni_{1/3}Co_{1/3}Mn_{1/3}]CO_3$ is presented in Fig. 1. The co-precipitated carbonate $[Ni_{1/3}Co_{1/3}Mn_{1/3}]CO_3$ has a typical hexagonal structure with a space group of *R-3c* corresponding to $MnCO_3$ (JCPDS No.

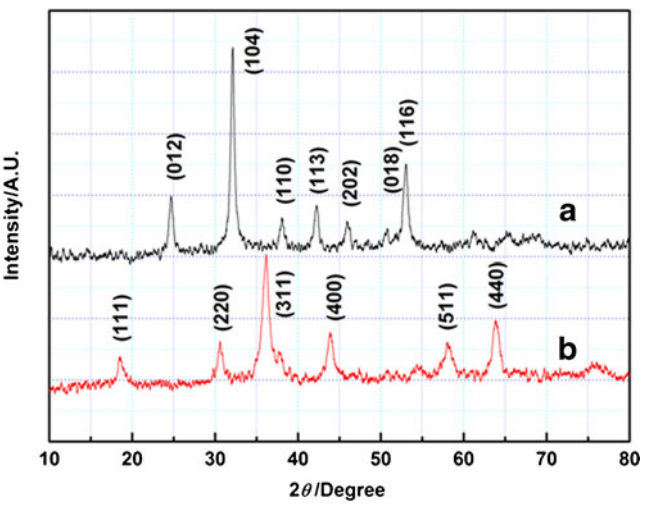

Fig. 1 XRD patterns of the precursor **a** $[Ni_{1/3}Co_{1/3}Mn_{1/3}]CO_3$ and **b** $[Ni_{1/3}Co_{1/3}Mn_{1/3}]_3O_4$

44–1472) [18]. The $[Ni_{1/3}Co_{1/3}Mn_{1/3}]CO_3$ was fired at 500 °C for 5 h to form $[Ni_{1/3}Co_{1/3}Mn_{1/3}]_3O_4$; the hexagonal carbonate structure changed to a cubic spinel Co_3O_4 structure during this process [28]. Figure 2 shows the SEM images of the precursor $[Ni_{1/3}Co_{1/3}Mn_{1/3}]CO_3$ and $[Ni_{1/3}Co_{1/3}Mn_{1/3}]_3O_4$. As shown in Fig. 2a, $[Ni_{1/3}Co_{1/3}Mn_{1/3}]CO_3$ powers are composed of well-dispersed spherical particles with an average size of about 10–15 μm. After firing at 500 °C for 5 h, the obtained precursor $[Ni_{1/3}Co_{1/3}Mn_{1/3}]_3O_4$ maintains the uniform spherical morphology of $[Ni_{1/3}Co_{1/3}Mn_{1/3}]CO_3$ (in Fig. 2b), and still shows excellent fluidity and dispersivity. The chemical compositions of the precursor powders are analyzed by atomic absorption spectroscopy. It was found that the Ni/Mn/Co ratios for sample $[Ni_{1/3}Co_{1/3}Mn_{1/3}]CO_3$ and $[Ni_{1/3}Co_{1/3}Mn_{1/3}]_3O_4$ are 0.335:0.334:0.331 and 0.334:0.332:0.332, respectively, which are almost the same as the designed values.

The XRD patterns of $Li[Ni_{1/3}Co_{1/3}Mn_{1/3}]O_2$ powders prepared from $LiOH{\cdot}H_2O$, Li_2CO_3, $CH_3COOLi{\cdot}2H_2O$, and $LiNO_3$ are presented in Fig. 3. As shown in Fig. 3, all samples can be indexed to the hexagonal α-$NaFeO_2$ structure (space group: $R\bar{3}m$) without any impurity peaks. The splits in the (006)/(102) and (108)/(110) doublets are observed in all XRD patterns, indicating that the layered $Li[Ni_{1/3}Co_{1/3}Mn_{1/3}]O_2$ cathode materials have been successfully synthesized from different Li sources. According to the XRD patterns, the structure parameters of *a*, *c*, *V*, *c*/*a* and I_{003}/I_{104} were calculated and are tabulated in Table 1. As shown in Table 1, the lattice parameters *a*, *c*, *c*/*a* and *V* of samples synthesized from different Li sources have scarcely any apparent change. There are, however, some different characteristics in the ratio of I_{003}/I_{104}. It is well known that the integrated intensity ratio of I_{003}/I_{104} (*R*) is sensitive to the cation mixing and is usually taken as a measure of the amount of the cation mixing in the series of $LiNiO_2$ families [29]. $R<1.2$ is an indication of undesirable cation mixing [30]. As shown in Table 1, the I_{003}/I_{104} values of all samples in this experiment are larger than 1.2, suggesting that small undesirable cation mixing exists in these samples [31].

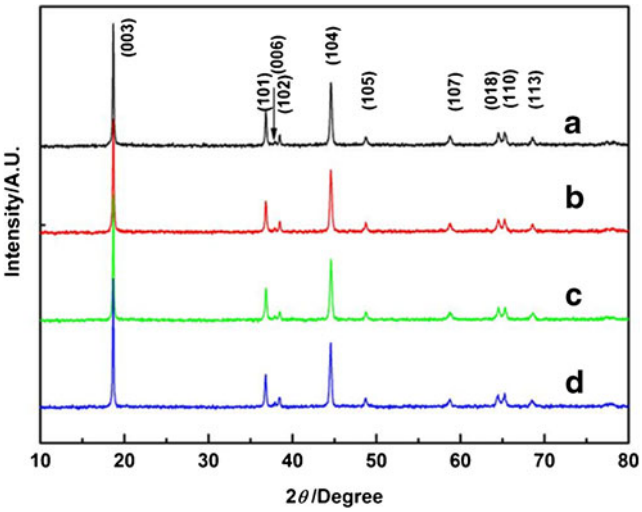

Fig. 3 XRD patterns of $Li[Ni_{1/3}Co_{1/3}Mn_{1/3}]O_2$ powders. **a** Sample A, **b** sample B, **c** sample C, and **d** sample D

It is well known that the particle size, particle size distribution and morphology of the sample will directly influence the electrochemical performance of the electrode materials. Figure 4 shows the SEM images of $Li[Ni_{1/3}Co_{1/3}Mn_{1/3}]O_2$ samples obtained from different Li sources. Figure 4a and b illustrates that the secondary particles of the $Li[Ni_{1/3}Co_{1/3}Mn_{1/3}]O_2$ samples prepared from $LiOH{\cdot}H_2O$ and Li_2CO_3 show the uniform spherical morphology, and each of the spherical particles consists of a large number of primary grains with submicron size. By comparison, the secondary particles of the samples obtained from $CH_3COOLi{\cdot}2H_2O$ and $LiNO_3$ appear non-homogeneous spherical morphology as shown in Fig. 4c and d. Previous reports by Ren et al. [20] and Cheralathan et al. [32] have shown that the uniform particle distribution of cathode materials could lead to the uniform depth of charge (DOC) of each particle, which increases the utilization of the material to enhance the overall battery performance. In addition, it is shown Table 1 that Li source can also affect the tap density of the final product $Li[Ni_{1/3}Co_{1/3}Mn_{1/3}]O_2$. The tap density of the sample A prepared from $LiOH{\cdot}H_2O$ reaches 2.32 $g cm^{-3}$, which is higher than those of sample

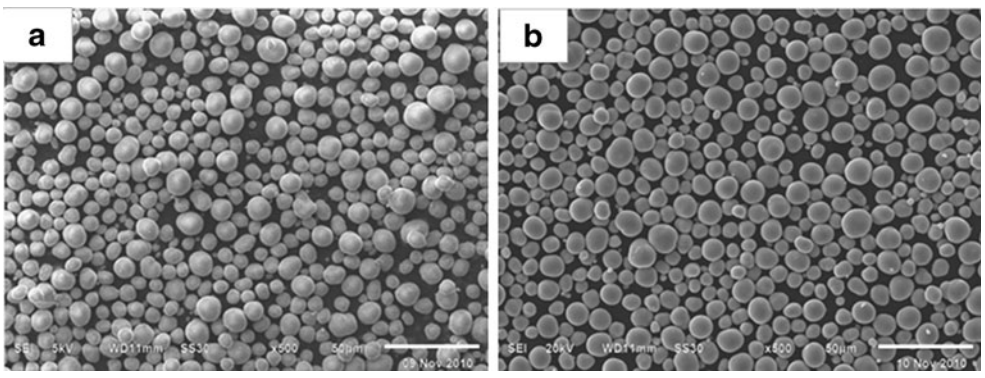

Fig. 2 SEM images of the precursor **a** $[Ni_{1/3}Co_{1/3}Mn_{1/3}]CO_3$ and **b** $[Ni_{1/3}Co_{1/3}Mn_{1/3}]_3O_4$

Table 1 Calculated structure parameters and tap densities for the final product $Li[Ni_{1/3}Co_{1/3}Mn_{1/3}]O_2$

Sample	a (Å)	c (Å)	V (Å^3)	c/a	I_{003}/I_{104}	Tap density (g cm^{-3})
Sample A	2.858	14.248	100.785	4.985	1.780	2.32
Sample B	2.859	14.251	100.877	4.985	1.668	2.17
Sample C	2.857	14.248	100.715	4.987	2.024	1.97
Sample D	2.861	14.258	101.068	4.984	1.987	1.84

B (2.17 gcm^{-3}), sample C (1.97 gcm^{-3}), and sample D (1.84 gcm^{-3}); meanwhile, this value is also higher than most $Li[Ni_{1/3}Co_{1/3}Mn_{1/3}]O_2$ materials prepared by carbonate co-precipitation method in previous reports [21–23]. The higher tap density of sample obtained from $LiOH{\cdot}H_2O$ can be attributed to the closer packing properties of the spherical particles compared to other samples [33].

Different Li sources result in different crystal structure and morphology of the $Li[Ni_{1/3}Co_{1/3}Mn_{1/3}]O_2$ materials, and will further affect their electrochemical performance. In order to study the influence of Li source on the rate capability of $Li[Ni_{1/3}Co_{1/3}Mn_{1/3}]O_2$, the cells were assembled and charged galvanostatically to 4.3 V with a 0.2C rate (32 mA g^{-1}) before each discharge testing, then discharged to 3.0 V at different C rates, from 0.2 to 5 C rates stepwise. The initial charge/discharge curves of the $Li[Ni_{1/3}Co_{1/3}Mn_{1/3}]O_2$ samples at 0.2C are presented in Fig. 5. The comparative discharge curves of $Li[Ni_{1/3}Co_{1/3}Mn_{1/3}]O_2$ samples at 0.2, 0.5, 1, 2, 5C are shown in Fig. 6, and the corresponding discharge capacity values are listed in Table 2. As shown in Fig. 5, samples A, B, C, and D deliver the initial charge/discharge capacities of 190.8/165.8, 187.7/162.2, 201/173.2, and 196/170.7 mA h g^{-1}, respectively, at 0.2C. Although sample C and sample D show high initial discharge capacity at 0.2C, the discharge capacity and average discharging voltage of these samples decrease quickly with increasing current density. The capacity of sample C maintains 90.8%, 82.9% and 71.3% at 1, 2 and 5C, respectively, compared with the specific capacity of 173.2 mA h g^{-1} at 0.2C; yet the capacity of sample D remains 90%, 81.2% and 69.1% at 1, 2 and 5C, respectively, compared with the specific capacity of 170.7 mA h g^{-1} at 0.2C. By contrast, sample A and sample B prepared from $LiOH{\cdot}H_2O$ and Li_2CO_3 show relatively

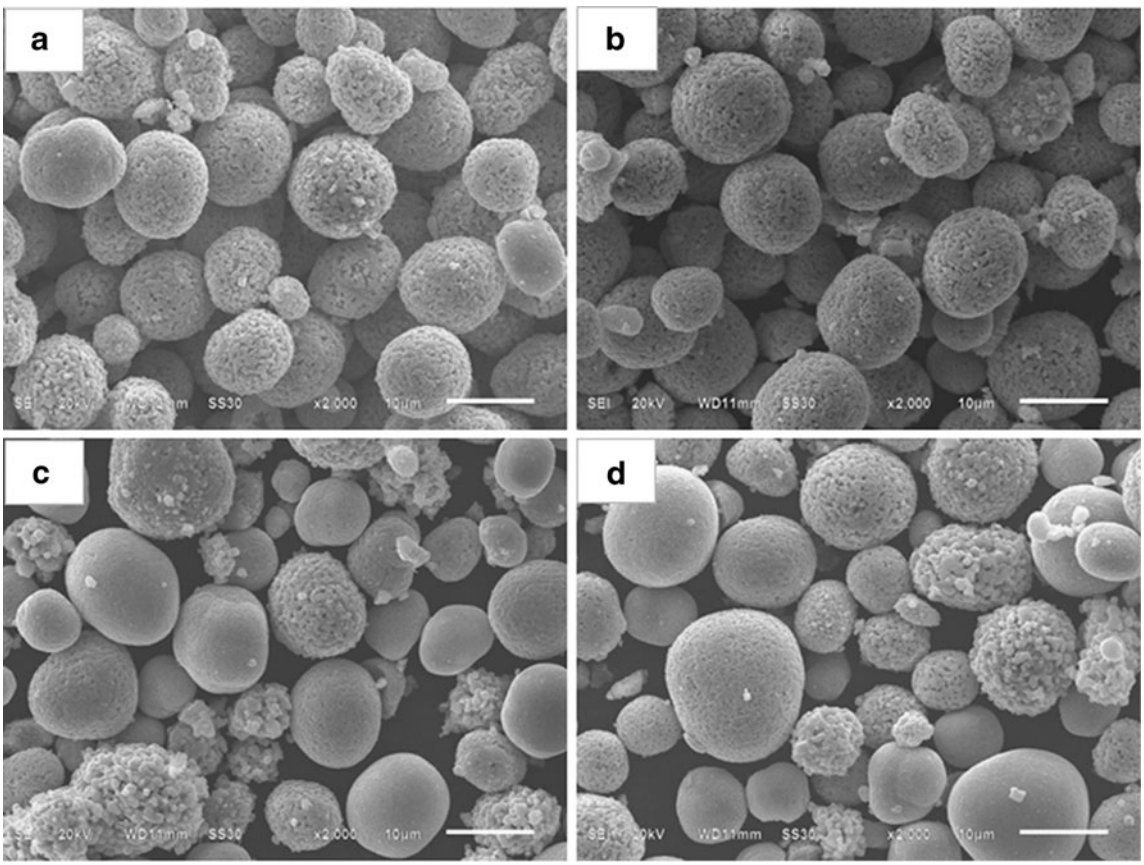

Fig. 4 SEM images of the $Li[Ni_{1/3}Co_{1/3}Mn_{1/3}]O_2$ materials. **a** Sample A, **b** sample B, **c** sample C, and **d** sample D

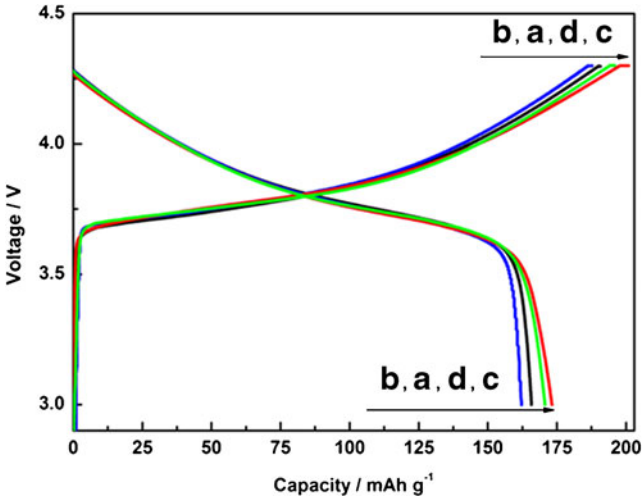

Fig. 5 The initial charge/discharge profiles of $Li[Ni_{1/3}Co_{1/3}Mn_{1/3}]O_2$ materials at 0.2C rate between 3.0 and 4.3 V at 25 °C. **a** Sample A, **b** sample B, **c** sample C, and **d** sample D

lower discharge capacity than the above two materials at 0.2C; however, they retain a high percentage of discharge capacity at high charge/discharge rate during the cycling process. The capacity of sample A retains 92.5%, 88.6% and 78% at 1, 2 and 5C, respectively,

Table 2 Discharge capacities of $Li[Ni_{1/3}Co_{1/3}Mn_{1/3}]O_2$ materials at various C rates

Sample	Discharge capacities at various C rates (mA hg^{-1})				
	0.2C	0.5C	1C	2C	5C
Sample A	165.8	158.5	153.3	143.6	129.3
Sample B	162.2	157.0	152.1	142.5	132.0
Sample C	173.2	165.6	157.3	143.6	123.3
Sample D	170.7	161.9	153.2	138.2	117.6

compared with the specific capacity of 165.8 mA h g^{-1} at 0.2C. Sample B delivers a discharge capacity of 152.1 mA h g^{-1} at 1C (the capacity retention rate is about 93.8% of that of 0.2C) and 142.5 mA h g^{-1} at 2C (the capacity retention rate is about 87.9% of that of 0.2C). Even at 5C (800 mA g^{-1}), the capacity of sample B is still as high at 132 mA h g^{-1} and the capacity retention rate is about 81.5% of that of 0.2C. In addition, it is noted that the discharge voltage drop of the sample B during high rate discharge is much smaller compared to the other three materials, and the operation voltage is more abruptly decayed at the end of discharge, suggesting that the better reversibility during Li de-intercalation processes occurs

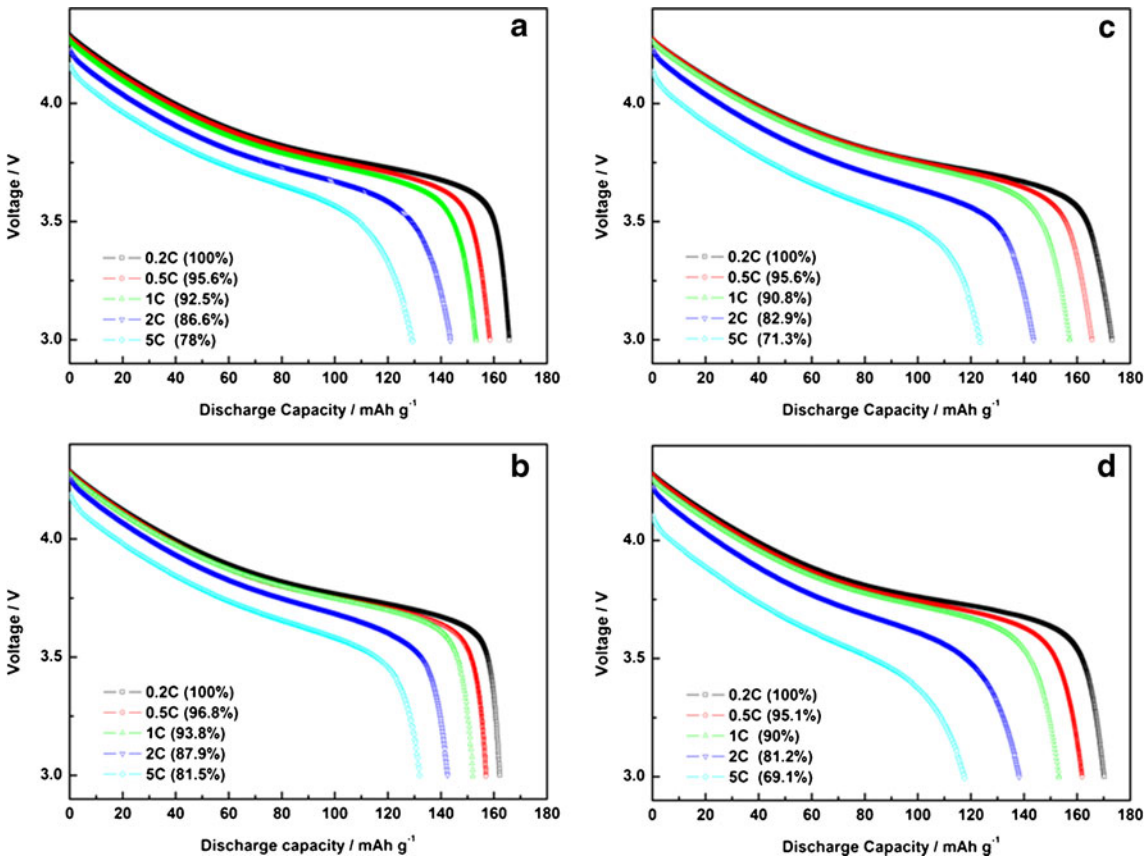

Fig. 6 Typical discharge curves for $Li[Ni_{1/3}Co_{1/3}Mn_{1/3}]O_2$ materials: **a** sample A, **b** sample B, **c** sample C, and **d** sample D at 0.2, 0.5, 1, 2, and 5C rates between 3.0 and 4.3 V at 25 °C

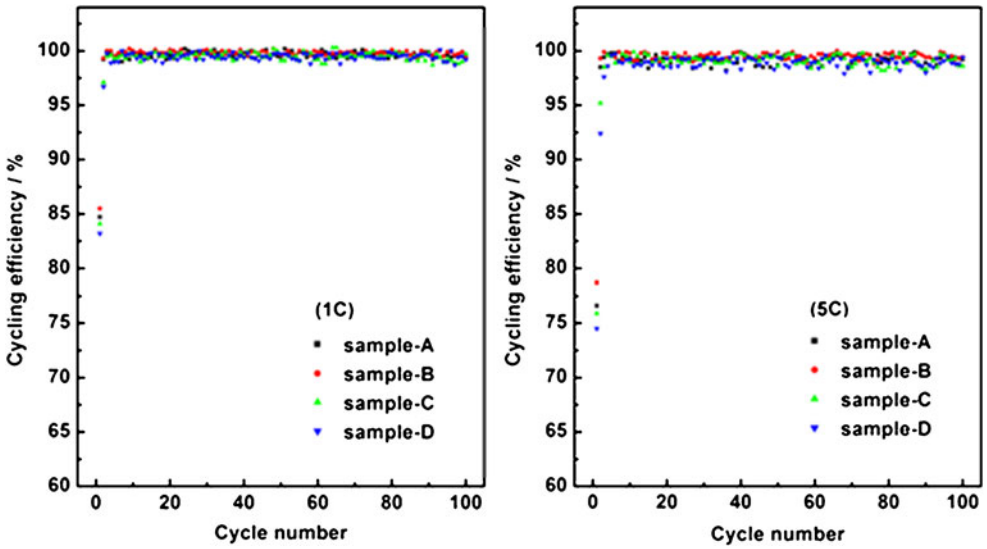

Fig. 7 Cycling efficiency as a function of cycle number for the $Li[Ni_{1/3}Co_{1/3}Mn_{1/3}]O_2$ materials at 1 and 5C rates at 25 °C

for sample B, which in turn, ensures a reduced capacity fade during battery cycling at high charge/discharge rate [33]. The rate capability of the as-prepared $Li[Ni_{1/3}Co_{1/3}Mn_{1/3}]O_2$ is possibly in connection with the conformation of spherical secondary particles. The uniform spherical particles could better accommodate intercalation/deintercalation of lithium ions during the charge/discharge process at high current rate, which results in a better rate capability [34].

To observe the influence of Li source on cycling properties at high C rates, the cells were measured at 1 and 5C rates in the voltage range of 3.0 and 4.3 V at 25 °C. Cycling efficiencies and discharge capacities of $Li[Ni_{1/3}Co_{1/3}Mn_{1/3}]O_2$ materials prepared by different Li sources as function of cycle number are presented in Figs. 7 and 8, respectively. It can be seen from Fig. 7 that all the samples show the high cycling efficiency upon charge and discharge cycling at 1 and 5C rates. Average efficiencies per cycle (excluding the first

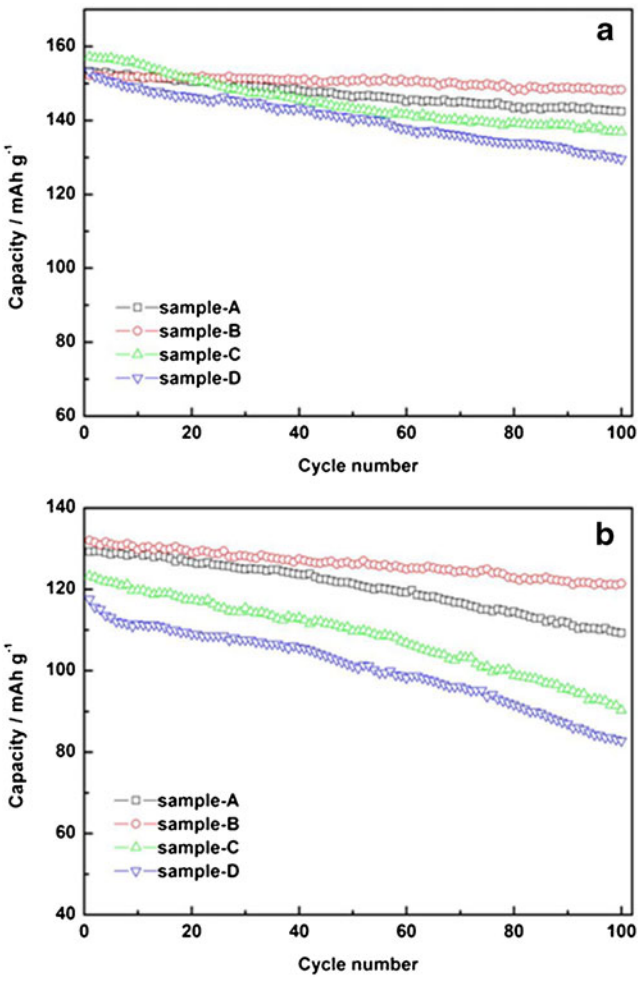

Fig. 8 Special discharge capacities as a function of cycle number for the $Li[Ni_{1/3}Co_{1/3}Mn_{1/3}]O_2$ materials at 1C rate (**a**) and 5C rate (**b**) at 25 °C

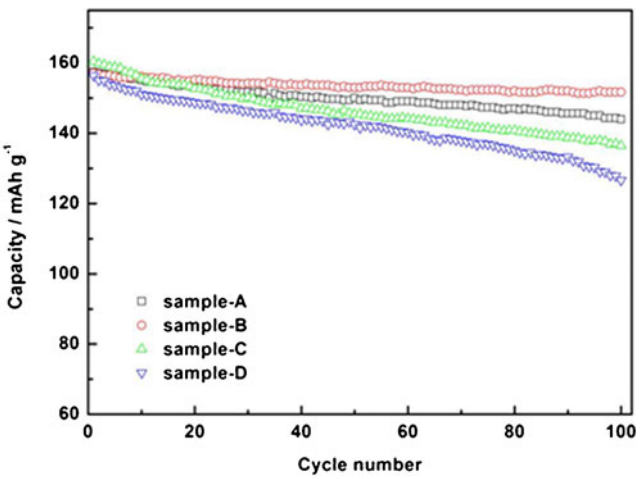

Fig. 9 Special discharge capacities as a function of cycle number for the $Li[Ni_{1/3}Co_{1/3}Mn_{1/3}]O_2$ materials at 1C rate at 55 °C

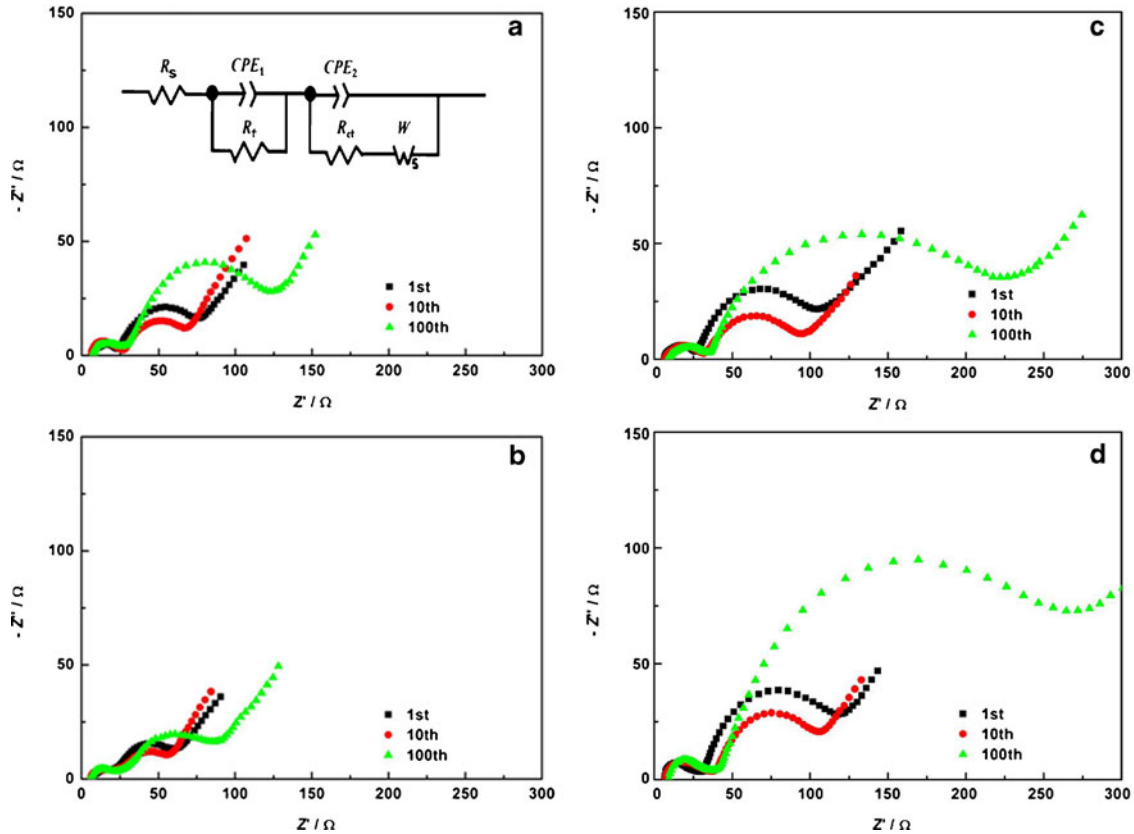

Fig. 10 Nyquist plots of **a** sample A, **b** sample B, **c** sample C, and **d** sample D at different cycle stages. *Insert*: schematic representation of equivalent circuit

cycle) of samples A, B, C, and D reach 99.58%, 99.67%, 99.53%, 99.42% at 1C rate, and are maintained at 99.29%, 99.46%, 99.12%, 99.01%, respectively, even at 5C rate. Comparatively, the cycling efficiency of sample B prepared from Li_2CO_3 is higher than the other three samples, and it can hold relative steady upon cycling. As shown in Fig. 8, compared with other samples obtained from $LiOH{\cdot}H_2O$, $CH_3COOLi{\cdot}2H_2O$, and $LiNO_3$, which show only 93% (capacity fading rate is 0.07% per cycle), 87% (capacity fading rate is 0.13% per cycle) and 84.6% capacity retention ratios (capacity fading rate is 0.154% per cycle), respectively, the sample prepared from Li_2CO_3 exhibits superior cycling performance with capacity retention ratio of 97.5% (capacity fading rate is only 0.025% per cycle) after 100 charge/discharge cycles at 1C rate. Similarly, after 100 charge/discharge cycles at high rate of 5C, the sample prepared from Li_2CO_3 shows excellent cycling performance with capacity retention ratio of 92% (capacity fading rate is 0.08% per cycle); however, the other samples obtained from $LiOH{\cdot}H_2O$, $CH_3COOLi{\cdot}2H_2O$, and $LiNO_3$ show only 84.5% (capacity fading rate is 0.155% per cycle), 73.2% (capacity fading rate is 0.268% per cycle), and 70.4% capacity retention ratios (capacity fading rate is 0.296% per cycle), respectively. Among the four Li sources used in this work, Li_2CO_3 appears to be the best Li source for preparation $Li[Ni_{1/3}Co_{1/3}Mn_{1/3}]O_2$ with excellent cyclability, and this excellent capacity retention at a high current density is slightly better than previous results obtained for $Li[Ni_{1/3}Co_{1/3}Mn_{1/3}]O_2$ [10–12, 35].

As well as operation at room temperature, the performance of the material at elevated temperatures is important. Therefore, it is significantly critical to address the high-temperature

Table 3 Simulated parameters using equivalent circuit in Fig. 10a

	Sample A			Sample B			Sample C			Sample D		
	1st	10th	100th	1st	10th	100th	1st	10th	100th	1st	10th	100th
R_s (Ω)	6.2	6.6	7.6	5.9	6.0	6.5	6.5	7.1	9.2	6.6	7.3	9.5
R_f (Ω)	17.1	20.2	21.3	14.0	16.1	16.7	20.2	24.6	25.9	22.7	30.6	32.3
R_{ct} (Ω)	53.5	40.4	95.5	42.7	34.8	66.2	79.9	62.6	190.5	89.5	68.7	233.2

characteristics of the prepared $Li[Ni_{1/3}Co_{1/3}Mn_{1/3}]O_2$. Figure 9 presents the cycling performance of $Li[Ni_{1/3}Co_{1/3}Mn_{1/3}]O_2$ materials at 1C between 3.0 and 4.3 V at 55 °C. It can be seen that the reversible capacities for all samples increase when the cells were cycled at 55 °C. This phenomenon is consistent with previous results reported by Yabuuchi and Ohzuku [36], and they considered that the increase in rechargeable capacity should be attributed to the negative shift of reversible potential as a function of temperature, not the kinetic effect. In addition, all samples exhibited slightly low capacity retention as compared to room temperature. The capacity retentions of samples A, B, C, and D are 91.4% (capacity fading rate is 0.086% per cycle), 96.6% (capacity fading rate is 0.034% per cycle), 85% (capacity fading rate is 0.15% per cycle), and 80.9% (capacity fading rate is 0.191% per cycle), respectively. This higher capacity fading upon cycling could be due to the instability of the electrolyte at elevated temperature [37].

To explain the reason for the different cyclical stability of the $Li[Ni_{1/3}Co_{1/3}Mn_{1/3}]O_2$ prepared from different lithium sources, electrochemical impedance spectroscopy (EIS) was carried out for the four $Li[Ni_{1/3}Co_{1/3}Mn_{1/3}]O_2$ materials at different cycle numbers after being charged to 4.3 V. The corresponding Nyquist plots are given in Fig. 10. The intercept at the Z_{real} axis at high frequency refers to R_s, which includes electrolyte solution resistance, electric contacts resistance, and ion conductive resistance. The semicircle in the high frequency range is due to the surface film resistance (R_f); the semicircle in the middle frequency range reflects the charge transfer resistance (R_{ct}); and the sloping line in the lower frequency represents lithium-ion diffusion resistance in electrode bulk: the Warburg impedance. The non-linear least squares fitting procedure from Boukamp [38] was used to simulate the impedance data, the equivalent circuit is given in Fig. 10a, and the results are listed in Table 3. It can be seen that the R_s and R_f of all samples slightly increased with increasing in cycle numbers. However, in contrast to R_s and R_f trends, the R_{ct} of $Li[Ni_{1/3}Co_{1/3}Mn_{1/3}]O_2$ materials first decreased with the increase of cycle number during 1–10 cycles, and then increased to the comparatively large values after 100 cycles. Apparently, the increase in R_{ct} will hinder the electrochemical reaction of lithiation and delithiation, which lead to the corresponding capacity fading upon cycling [5]. In addition, it can be seen that sample B prepared from Li_2CO_3 shows the smallest total resistance (sum of surface layer resistance and charge transfer resistance) and relatively stable R_{ct} values upon charge and discharge cycles, which guarantees the best cyclability.

Conclusions

Spherical $Li[Ni_{1/3}Co_{1/3}Mn_{1/3}]O_2$ cathode materials have been successfully synthesized by continuous carbonate co-precipitation using different lithium sources. It has been found that different Li sources will result in differences in the crystal structure and morphology of $Li[Ni_{1/3}Co_{1/3}Mn_{1/3}]O_2$ spherical particles, and thus further affect its tap density, rate capability and high rate cycling performance. The samples obtained from $CH_3COOLi{\cdot}2H_2O$ and $LiNO_3$ show non-homogeneous spherical morphology with low tap densities and poor high rate cycling performance. Meanwhile, samples obtained from $LiOH{\cdot}H_2O$ and Li_2CO_3 appear to have uniform spherical morphology and show relative higher tap densities as well as better high rate cycling performance than the former two. Among the four Li sources used in this work, $LiOH{\cdot}H_2O$ proves to be the best Li source for synthesis $Li[Ni_{1/3}Co_{1/3}Mn_{1/3}]O_2$ with high tap density (2.32 $g cm^{-3}$), which is attributed to the closed packing properties of the spherical particles. Li_2CO_3 is appears to be the best Li source for preparation $LiNi_{1/3}Co_{1/3}Mn_{1/3}O_2$ with excellent rate capability and high rate cycling performance. The capacity retention percentage at 0.5, 1, 2 and 5C based on 0.2C reaches 96.8%, 93.8%, 87.9% and 81.5%, respectively. Upon extended cycling at 1 and 5C, 97.5% and 92% of the initial discharge capacity can be maintained after 100 cycles. The enhanced high rate cyclability of $Li[Ni_{1/3}Co_{1/3}Mn_{1/3}]O_2$ prepared from Li_2CO_3 is mainly attributed to the uniform distribution of the spherical particles, which led to small total resistance and relatively stable R_{ct} values during the cycling process.

Acknowledgements This work was financially supported by the National Natural Science Foundation of China under project No. 20871101, Joint Fund of Natural Science of Hunan Province and Xiangtan City under project No. 09BG005, Industrial Project of Colleges and Universities of Hunan Province under project No. 10CY005, Project of Condition Research of Hunan Province under project No. 2010TC2004 and Colleges and Universities in Hunan Province plans to graduate research and innovation under project No. CX2009B133.

References

1. Ohzuku T, Makimura Y (2001) Chem Lett 30:642–643
2. Hwang BJ, Yu TH, Cheng MY, Santhanam R (2009) J Mater Chem 19:4536–4544
3. Cho J, Manthiram A (2005) J Electrochem Soc 152:A1714–A1718
4. Wang L, Li JG, He XM, Pu WH, Wan CR, Jiang CY (2009) J Solid State Electrochem 13:1157–1164
5. Ni JF, Zhou HH, Chen JT, Zhang XX (2008) Electrochim Acta 53:3075–3083
6. Li J, Zheng JM, Yang Y (2007) J Electrochem Soc 154:A427–A432
7. Koyama Y, Tanaka I, Ohuzuku T (2003) J Power Sources 119–121:644–648
8. Kim JM, Chung HT (2004) Electrochim Acta 49:937–944
9. Luo XF, Wang XY, Liao L, Gamboab S, Sebastian PJ (2006) J Power Sources 158:654–658

10. Liang YG, Han XY, Zhou XW, Sun JT, Zhou YH (2007) Electrochem Commun 9:965–970
11. Santhanam R, Rambabu B (2010) J Power Sources 195:4313–4317
12. Santhanam R, Jones P, Sumana A, Rambabu B (2010) J Power Sources 195:7391–7396
13. Kanamura K, Koizumi S, Dokko K (2008) J Mater Sci 43:2138–2142
14. Song MY, Song J, Bang EY, Mumm DR (2009) Ceram Int 35:1625–1631
15. Yang TY, Sun KN, Lei ZY, Zhang NQ, Lang Y (2011) J Solid State Electrochem 15:391–397
16. Guo J, Jiao LF, Yuan HT, Li HX, Zhang M, Wang YM (2006) Electrochim Acta 51:3731–3735
17. Xia H, Wang HL, Xiao W, Lu L, Lai MO (2009) J Alloys and Compd 480:696–701
18. Zhang S, Deng C, Fu BL, Yang SY, Ma L (2010) Powder Technol 198:373–380
19. Deng C, Zhang S, Ma L, Sun YH, Yang SY, Fu BL, Liu FL, Wu Q (2011) J Alloys Compd 509:1322–1327
20. Ren HB, Huang YH, Wang YH, Li ZJ, Cai P, Peng ZH, Zhou YH (2009) Mater Chem Phys 117:41–45
21. Park S-H, Kang S-H, Belharouak I, Sun YK, Amine K (2008) J Power Sources 177:177–183
22. Zhang S, Deng C, Yang SY, Niu H (2009) J Alloys Compd 484:519–523
23. He P, Wang HR, Qi L, Osaka T (2006) J Power Sources 160:627–632
24. Yang SY, Wang XY, Chen QQ, Yang XK, Li JJ, Wei QL J Solid State Electrochem. doi:10.1007/s10008-011-1356-1
25. Shen BJ, Ma JS, Wu HC, Lu CH (2008) Mater Lett 62:4075–4077
26. Ren H, Wang Y, Li D, Ren L, Peng Z, Zhou Y (2008) J Power Sources 178:439–444
27. Lu CH, Lin YK (2009) J Power Sources 189:40–44
28. Park S-H, Shin H-S, Myung S-T, Yoon CS, Amine K, Sun Y-K (2005) Chem Mater 17:6–8
29. Reimers JN, Rossen E, Jones CD, Dahn JR (1993) Solid State Ionics 61:335–344
30. Li W, Reimers JN, Dahn JR (1993) Solid State Ionics 67:123–128
31. Delmas C, Saadoune I, Rougier A (1993) J Power Sources 44:595–602
32. Cheralathan KK, Kang NY, Park HS, Lee YJ, Choi WC, Ko YS, Park YK (2010) J Power Sources 195:1486–1494
33. Lee M-H, Kang Y-J, Myung S-T, Sun Y-K (2004) Electrochim Acta 50:939–948
34. Shin H-S, Park S-H, Bae YC, Sun Y-K (2005) Solid State Ionics 176:2577–2581
35. Liu L, Zhang NQ, Sun KN, Yang TY (2009) J Phys Chem Solids 70:727–731
36. Yabuuchi N, Ohzuku T (2005) J Power Sources 146:636–639
37. Shaju KM, Bruce PG (2007) J Power Sources 174:1201–1205
38. Boukamp BA (1989) Equivalent circuit, user's manual. University of Twente, The Netherlands